Electronic Supplementary Material (ESI) for Inorganic Chemistry Frontiers.

Supporting Information

A Dual Approach to Cancer Treatment: Gold(I) Terpyridine Derivatives as DNA Binders and Inhibitors of Mammalian Thioredoxin Reductase

María Gil-Moles,[a,b,c], M. Elena Olmos[b], José M. López-de-Luzuriaga*[b], Ingo Ott*[c] and M. Concepción Gimeno*[a]

[a] Departamento de Química Inorgánica, Instituto de Síntesis Química y Catálisis Homogénea (ISQCH), CSIC-Universidad de Zaragoza, 50009 Zaragoza, Spain
E-mail: gimeno@unizar.es

[b] Departamento de Química, Universidad de La Rioja. Instituto de Investigación en Química (IQUR). Complejo Científico-Tecnológico, 26004-Logroño, Spain.

E-mail: josemaria.lopez@unirioja.es

[c] Institute of Medicinal and Pharmaceutical Chemistry, Technische Universität Braunschweig, Beethovenstr. 55, 38106 Braunschweig, Germany

E-mail: ingo.ott@tu-bs.de

Table of contents

1 ^{1}H-NMR and ^{31}P{^{1}H} NMR Figures S1-S8

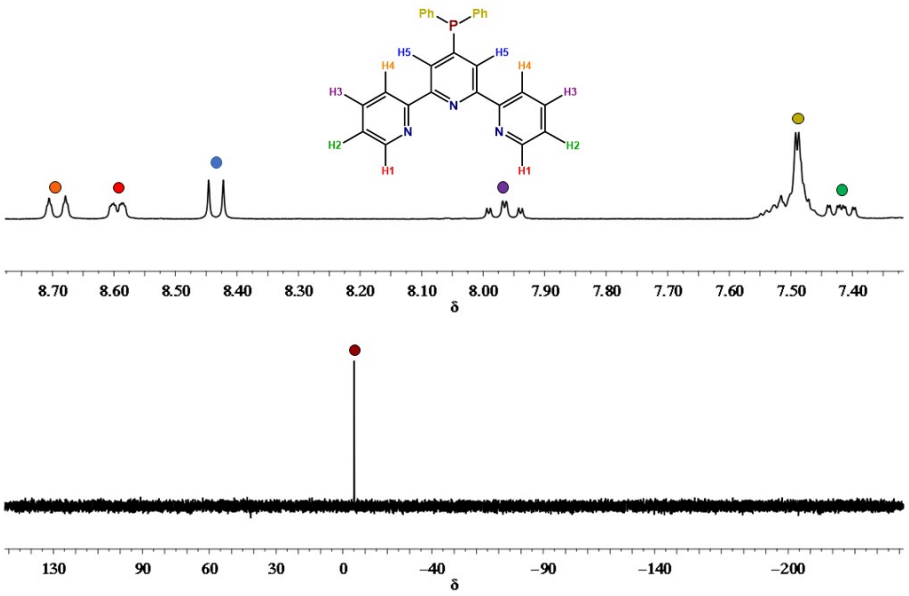

Figure S1: ^{1}H–RMN (400 MHz d_6–$(CH_3)_2O$). (up) and ^{31}P{^{1}H}–RMN (162 MHz d_6–$(CH_3)_2O$) (bottom) of 4´–PPh_2terpy

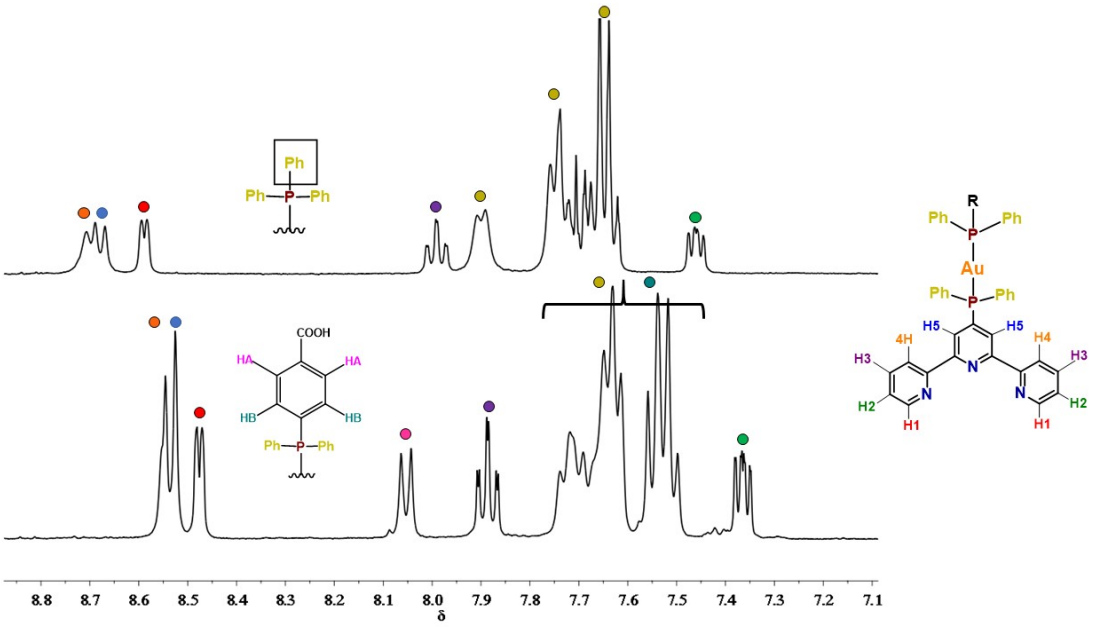

Figure S2: ^{1}H–RMN (400 MHz, d_6-$(CH_3)_2O$) of **1** (up) and **2** (bottom).

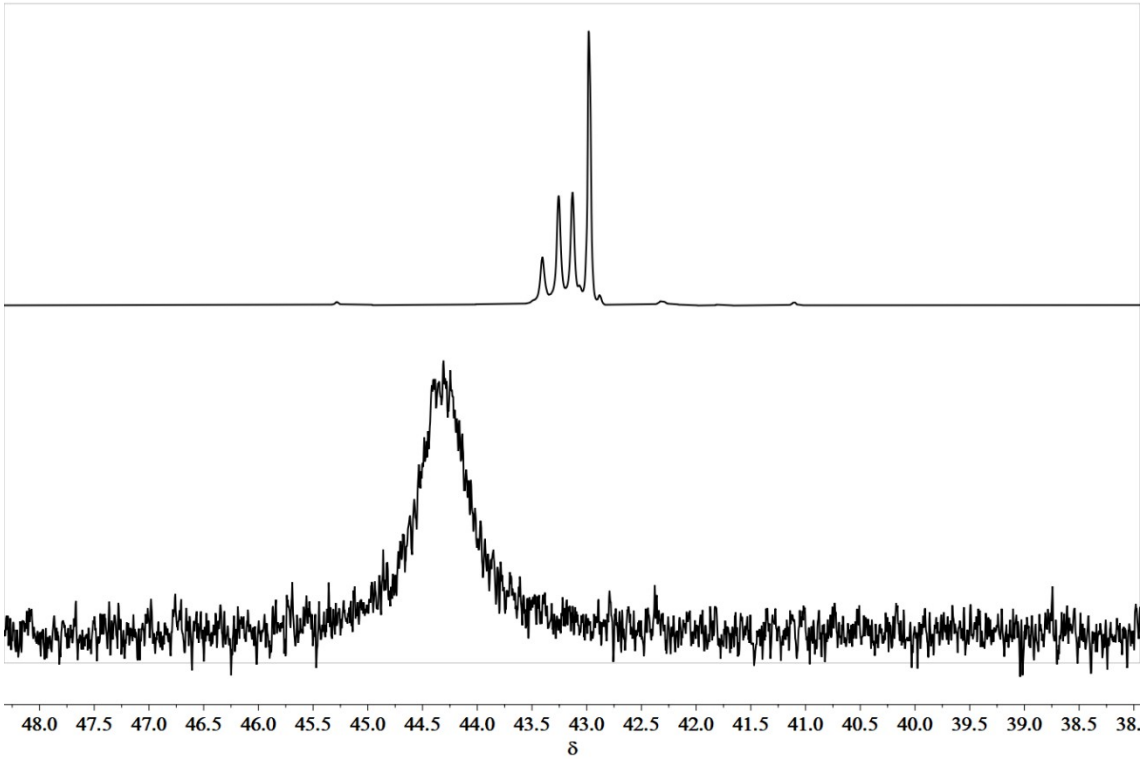

Figure S3: $^{31}P\{^{1}H\}$–RMN (162 MHz d_6-$(CH_3)_2O$) of **1** at 220K (up) and **1** at 298K (bottom).

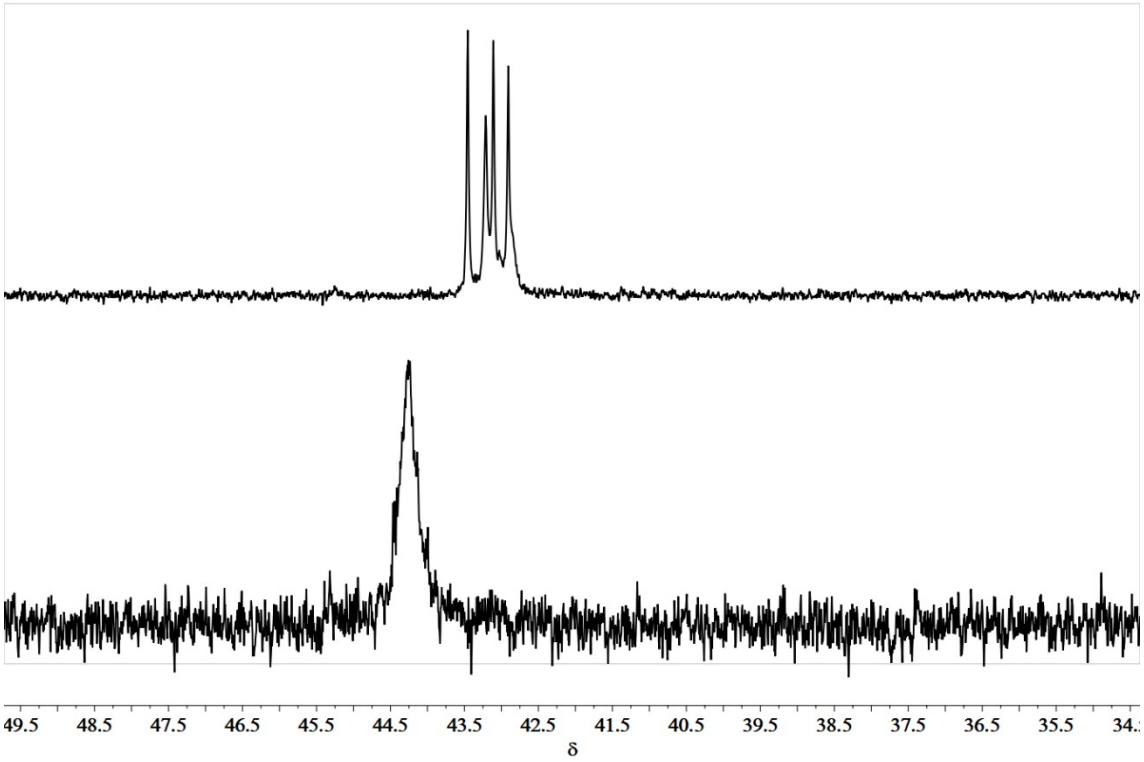

Figure S4: $^{31}P\{^{1}H\}$–RMN (162 MHz d_6-$(CH_3)_2O$) of **2** at 220K (up) and **2** at 298K (bottom).

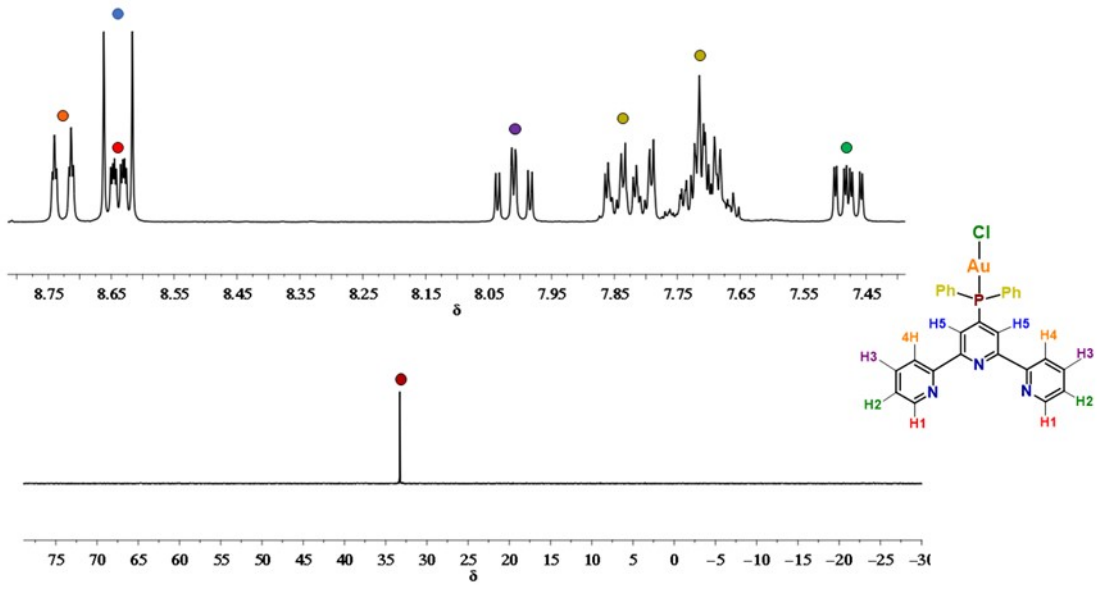

Figure S5: ^{1}H–RMN (400 MHz d_6–$(CH_3)_2O$). (up) and $^{31}P\{^{1}H\}$–RMN (162 MHz d_6–$(CH_3)_2O$) (bottom) of **3**.

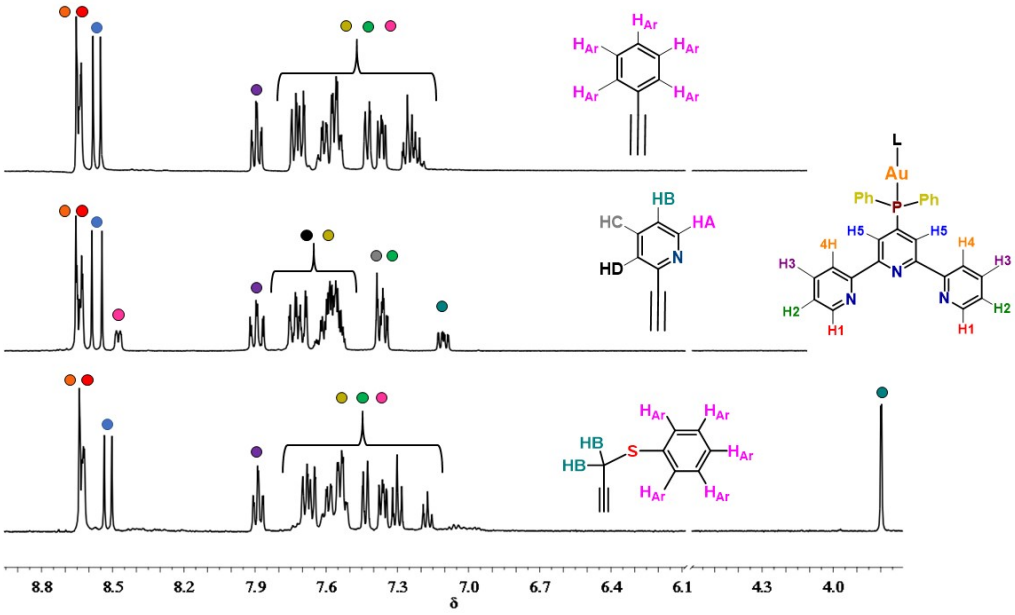

Figure S6: ^{1}H–RMN (400 MHz d_2–CH_2Cl_2) of **4** (up) **5** (middle)and **6** (bottom).

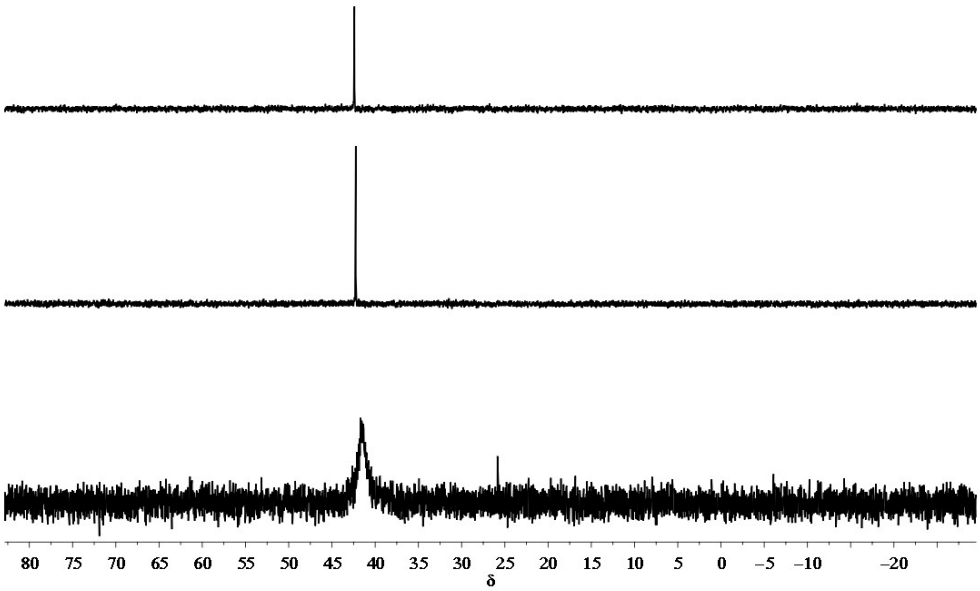

Figure S7: $^{31}P\{^{1}H\}$–RMN (162 MHz d_2–CH_2Cl_2) of **4** (up) **5** (middle)and **6** (bottom).

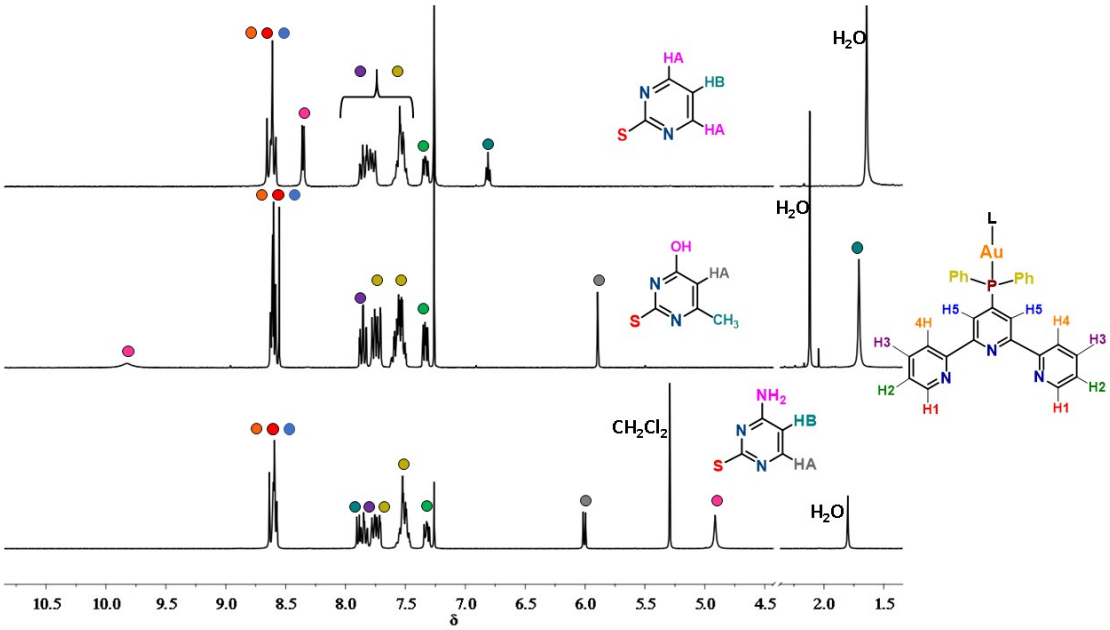

Figure S8: ^{1}H–RMN (400 MHz d_1–$CHCl_3$) of **7** (up) **8** (middle)and **9** (bottom).

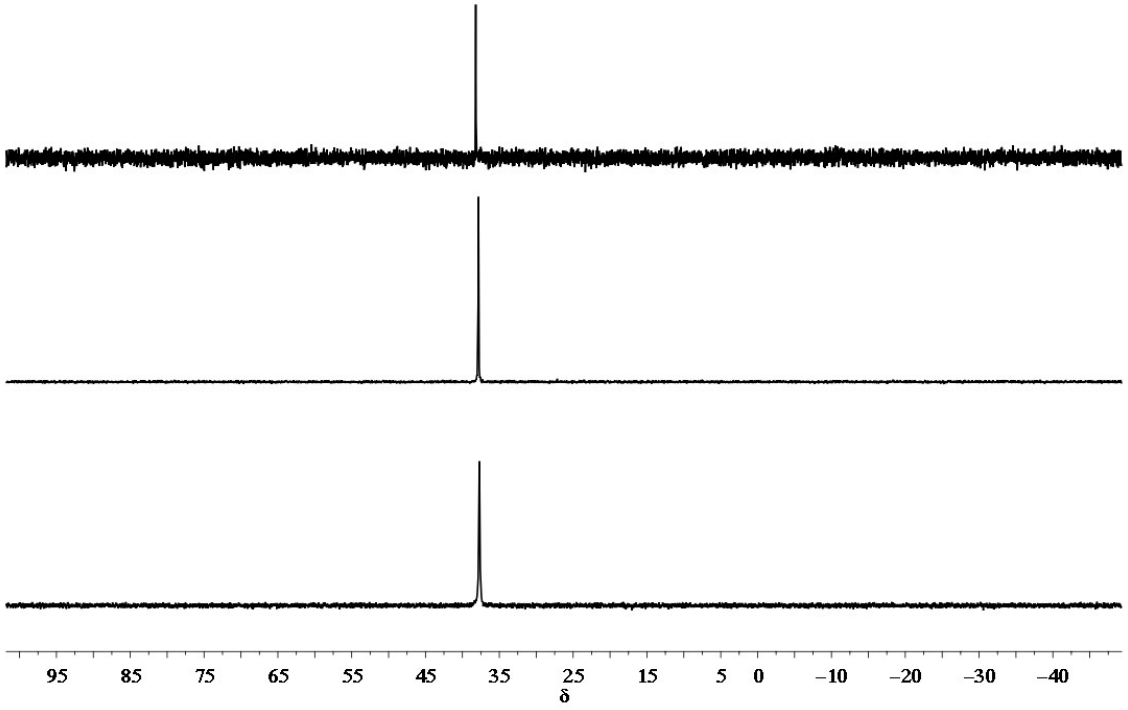

Figure S9: $^{31}P\{^{1}H\}$–RMN (162 MHz d_1–$CHCl_3$) of **7** (up) **8** (middle)and **9** (bottom).

2 Stability studies

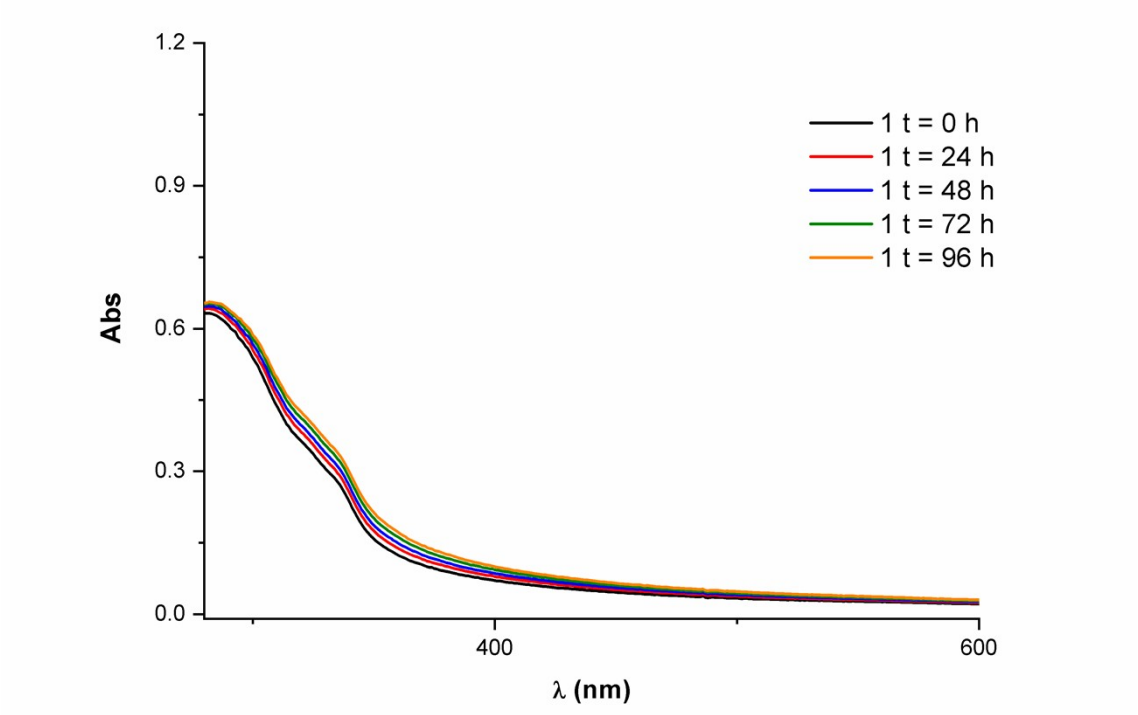

Figure S10: Stability study of **1** in a mixture of PBS/DMF (10%).

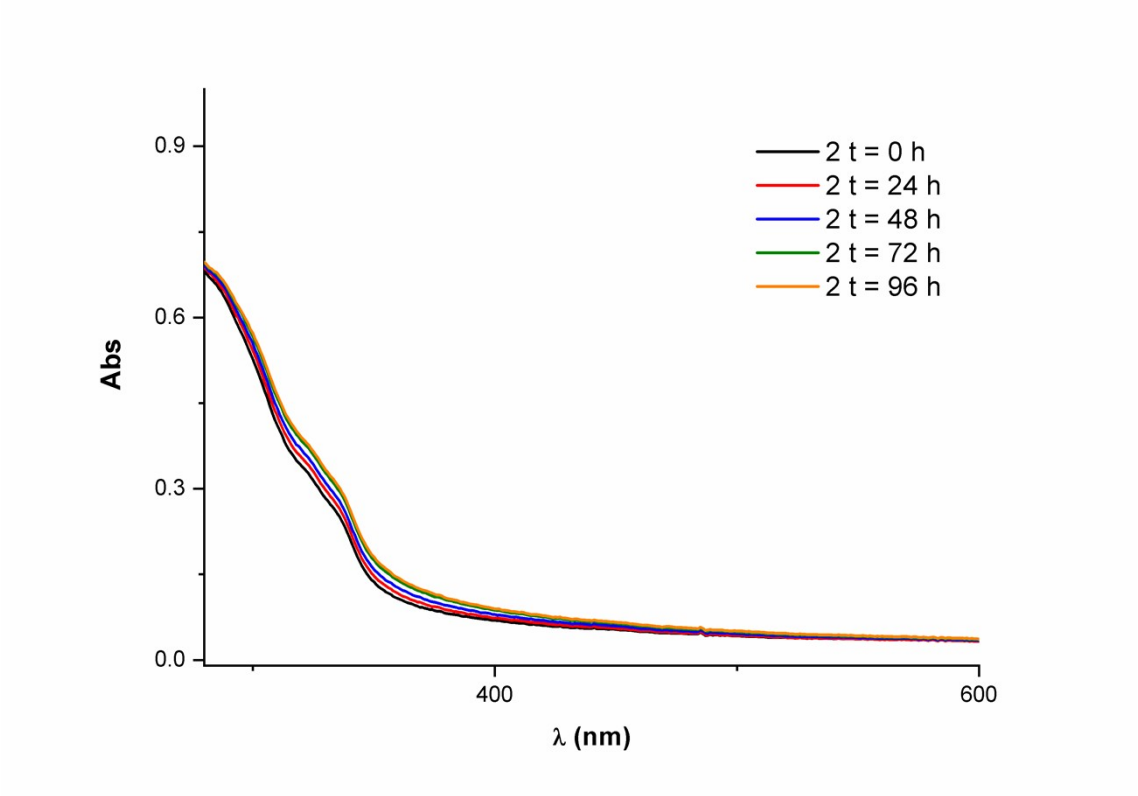

Figure S11: Stability study of **2** in a mixture of PBS/DMF (10%).

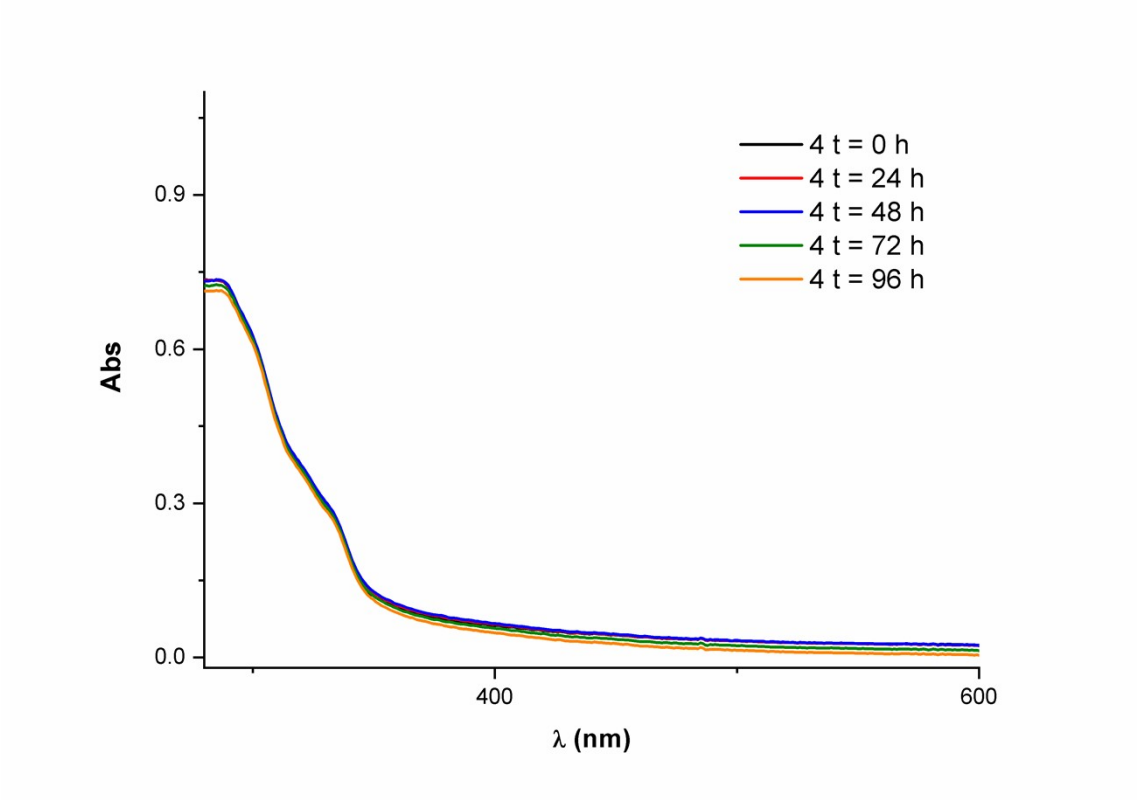

Figure S12: Stability study of **4** in a mixture of PBS/DMF (10%).

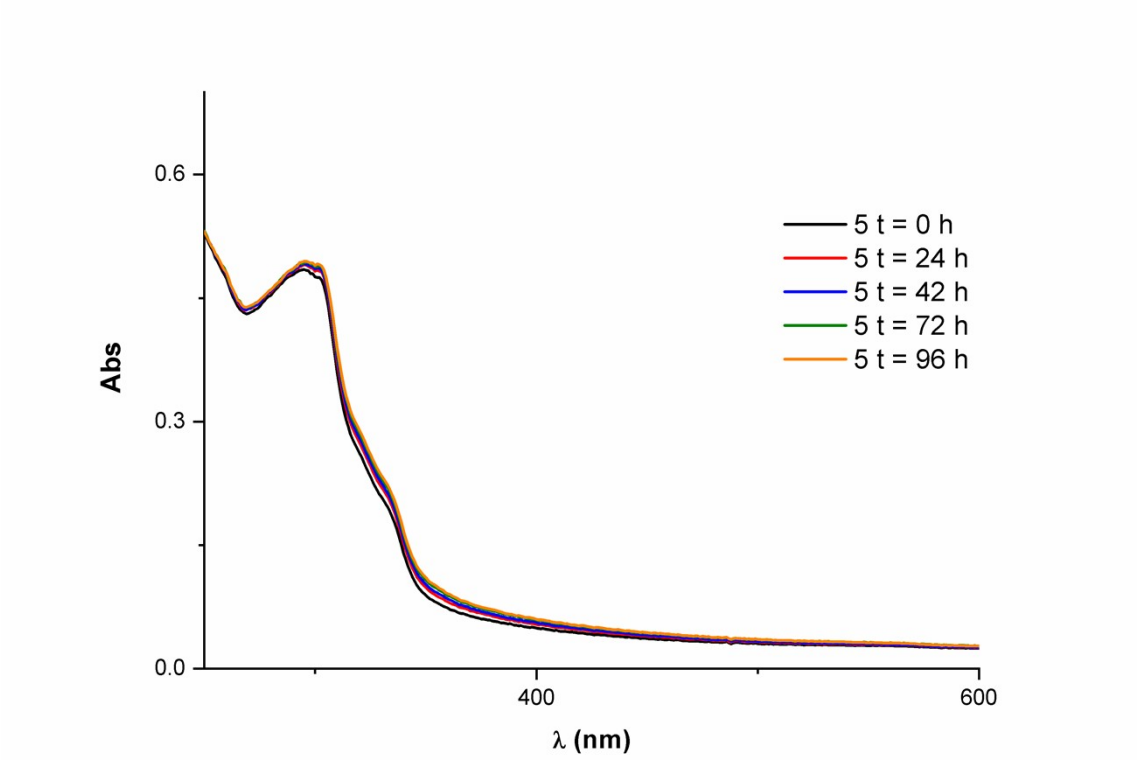

Figure S13: Stability study of **5** in a mixture of PBS/DMF (10%).

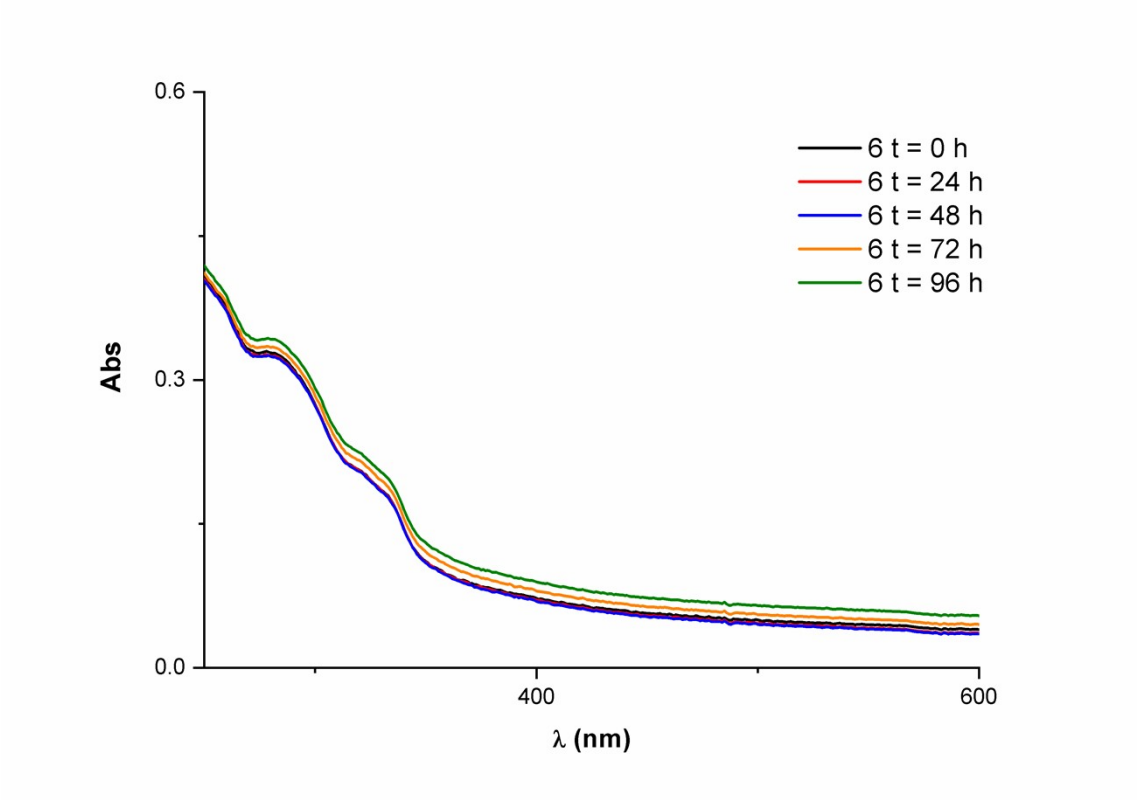

Figure S14: Stability study of **6** in a mixture of PBS/DMF (10%).

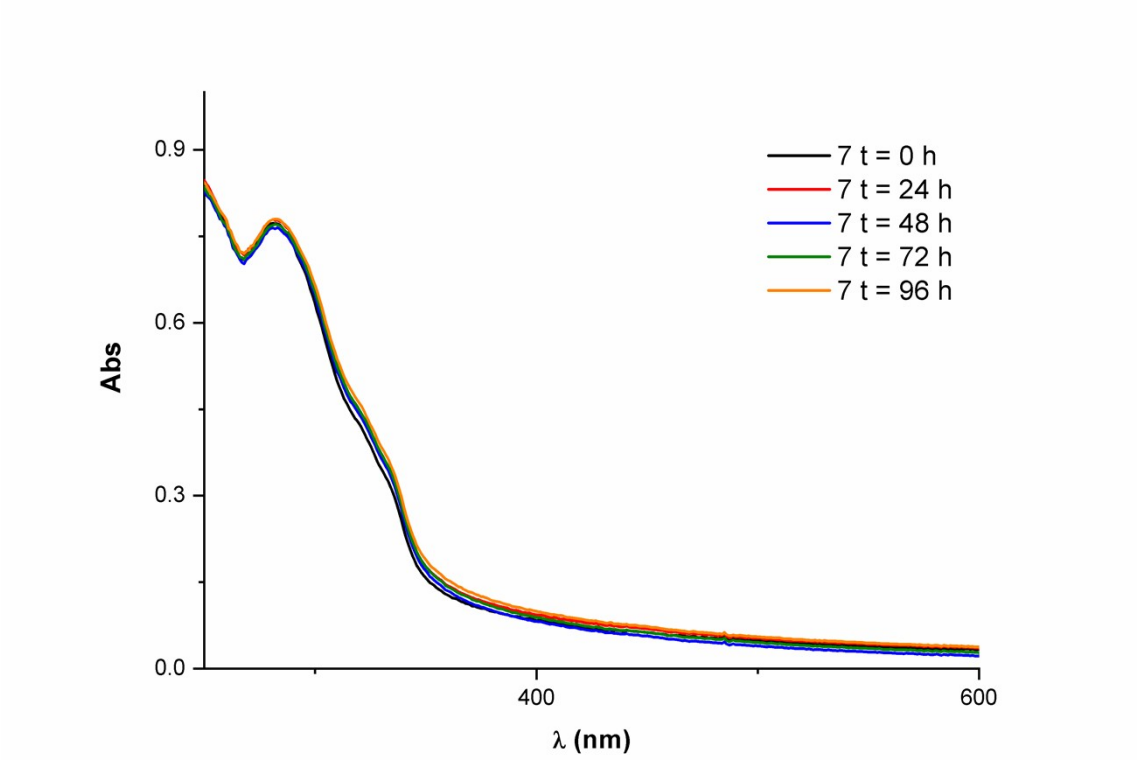

Figure S15: Stability study of **Au-7** in a mixture of PBS/DMF (10%).

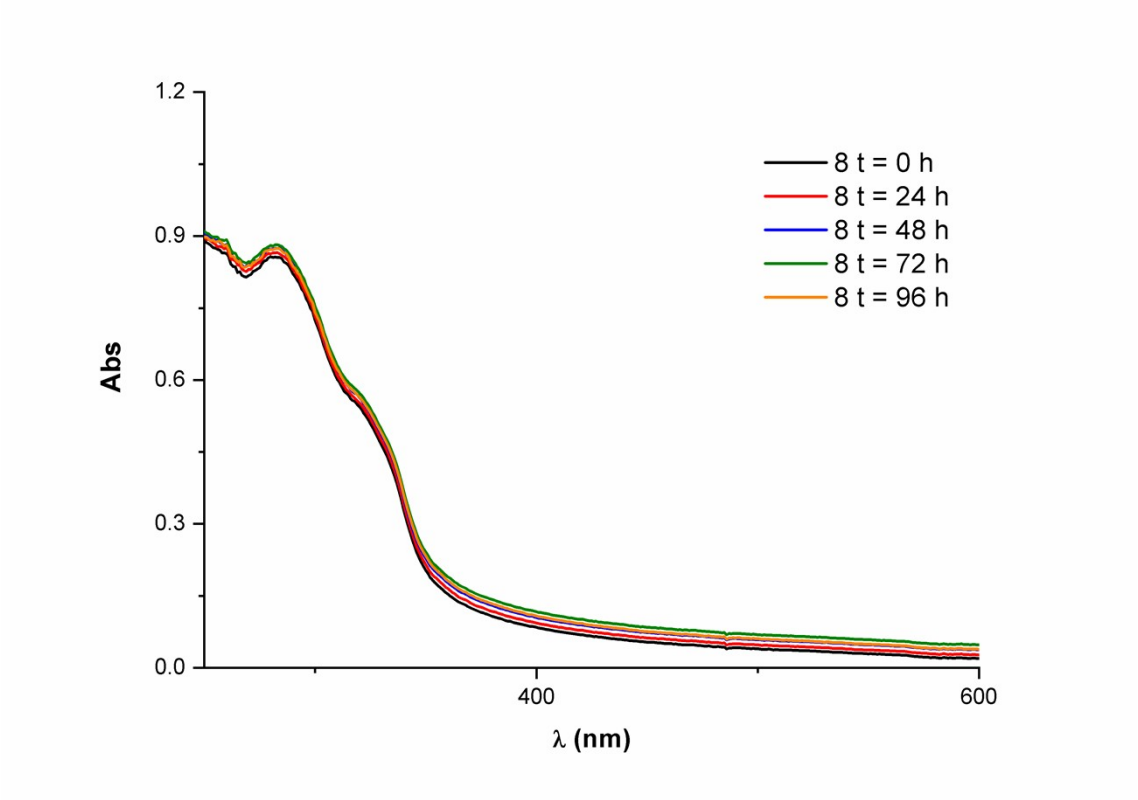

Figure S16: Stability study of **8** in a mixture of PBS/DMF (10%).

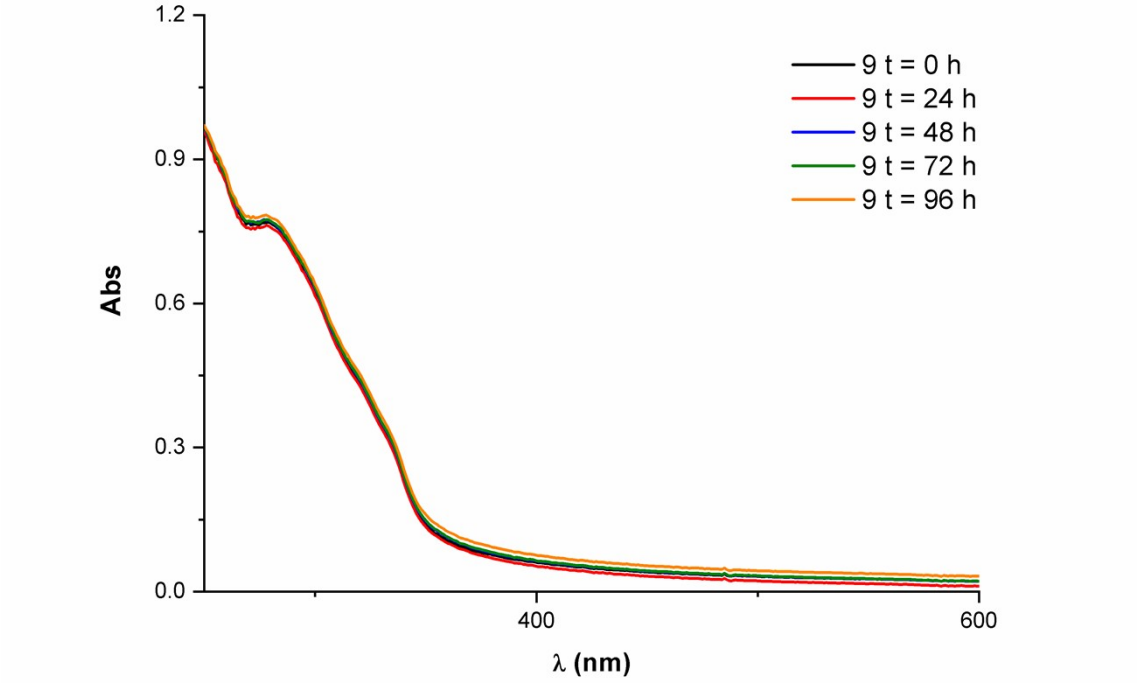

Figure S17: Stability study of **9** in a mixture of PBS/DMF (10%).

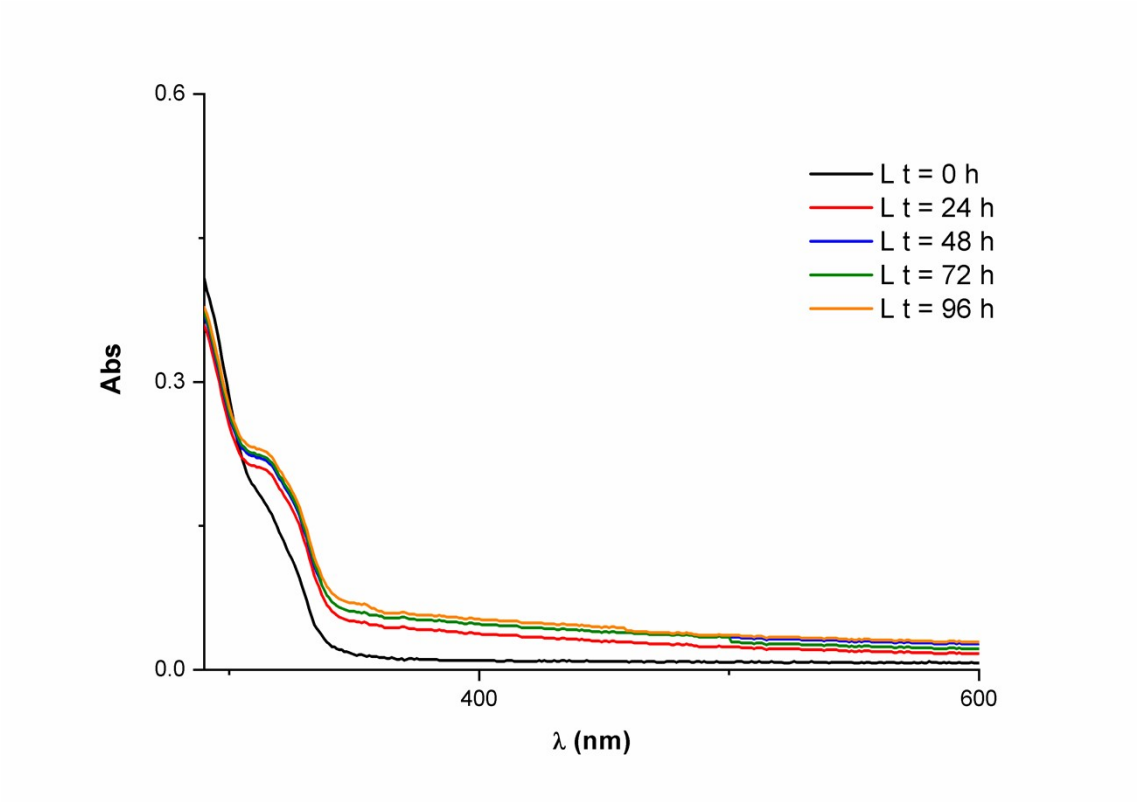

Figure S18: Stability study of **L** in a mixture of PBS/DMF (10%).

3 Ligand exchange reactions ^{1}H-NMR and ^{31}P{^{1}H} NMR

[Au(PPh$_2$(C$_6$H$_4$COOH))(4´–PPh$_2$terpy)]BF$_4$ (**2**)

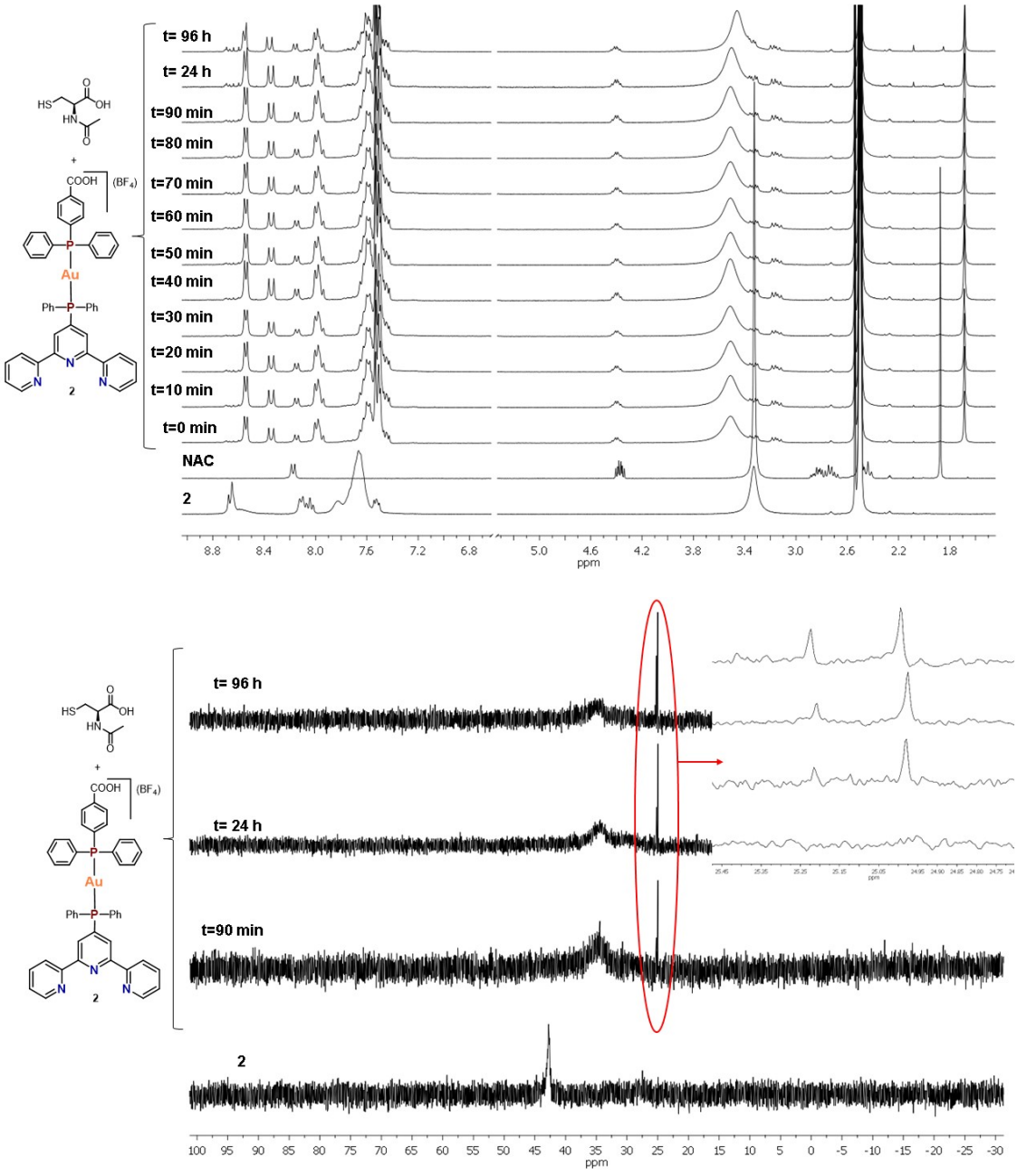

Figure S19: ^{1}H–RMN (300 MHz d$_6$–DMSO) (up) and ^{31}P{^{1}H}–RMN (121 MHz d$_6$–DMSO) (bottom) of **2** (10 mM) in presence of NAC (10 mM) at different times.

[AuCl(4´–PPh_2terpy)] (**3**)

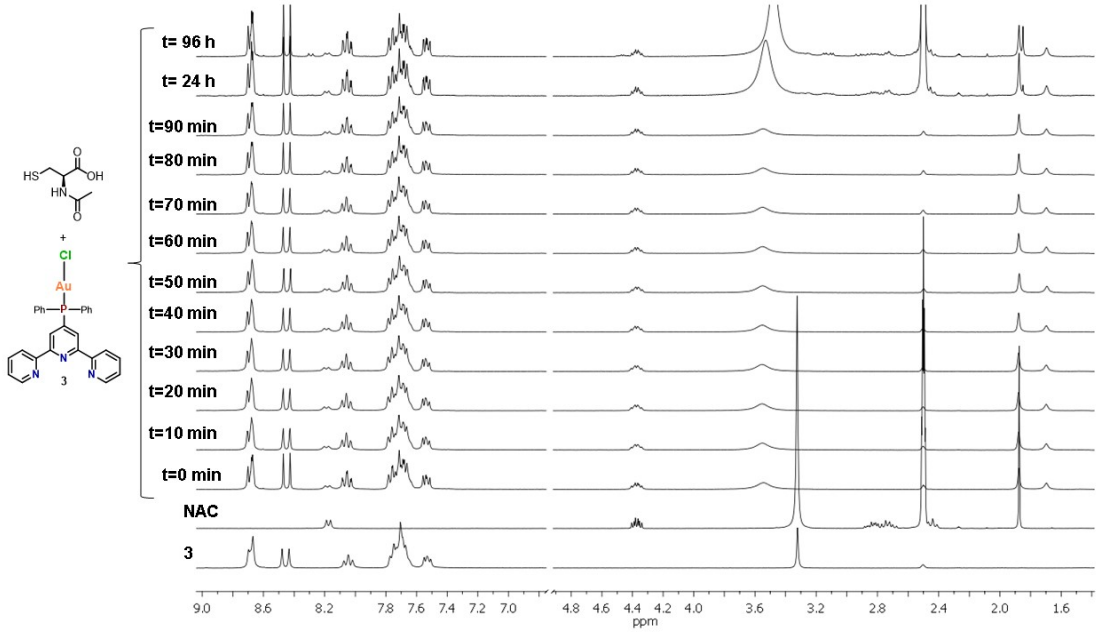

Figure S20: ^{1}H–RMN (300 MHz d_6–DMSO) of **3** (10 mM) in presence of NAC (10 mM) at different times.

[Au(C≡CPh)(4´–PPh_2terpy)] (**4**)

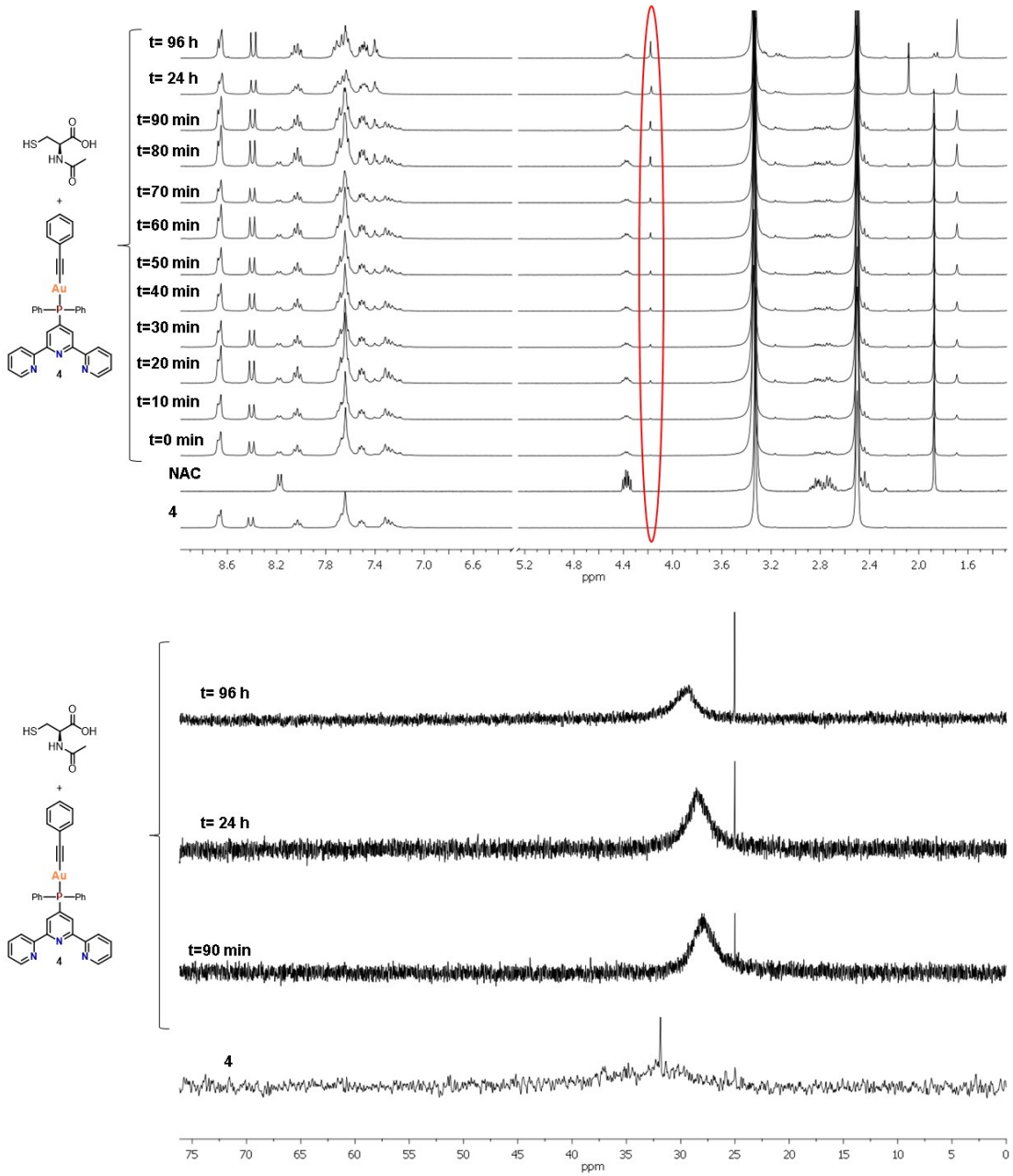

Figure S21: ^{1}H–RMN (300 MHz d_6–DMSO) (up) and $^{31}P\{^{1}H\}$–RMN (121 MHz d_6–DMSO) (bottom) of **4** in presence of NAC at different times.

[Au(SPyrim)(4´–PPh_2terpy)] (**7**):

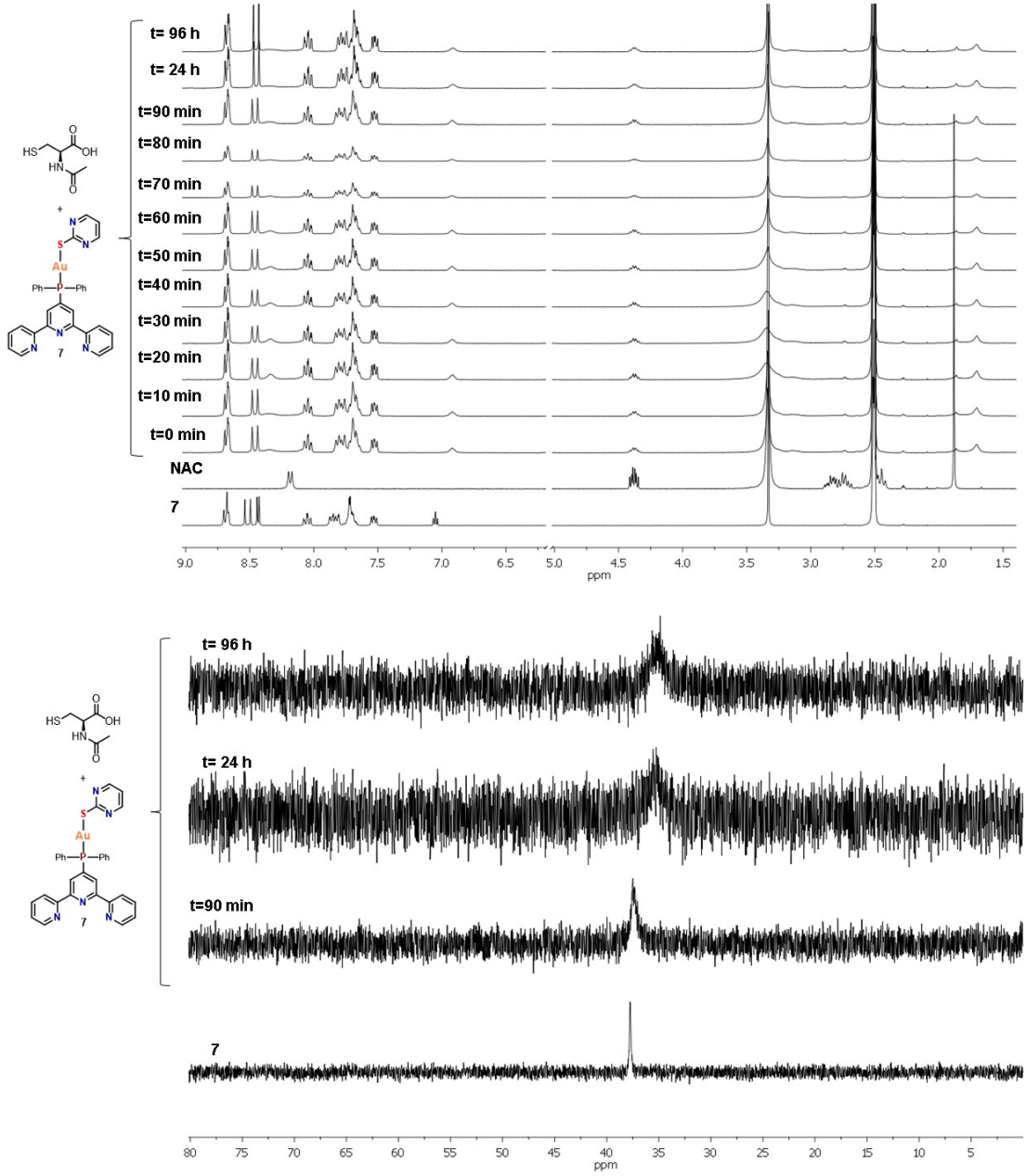

Figure S22: ^{1}H–RMN (300 MHz d_6–DMSO) (up) and $^{31}P\{^{1}H\}$–RMN (121 MHz d_6–DMSO) (bottom) of **7** in presence of NAC at different times.

4'-PPh_2terpy (**L**):

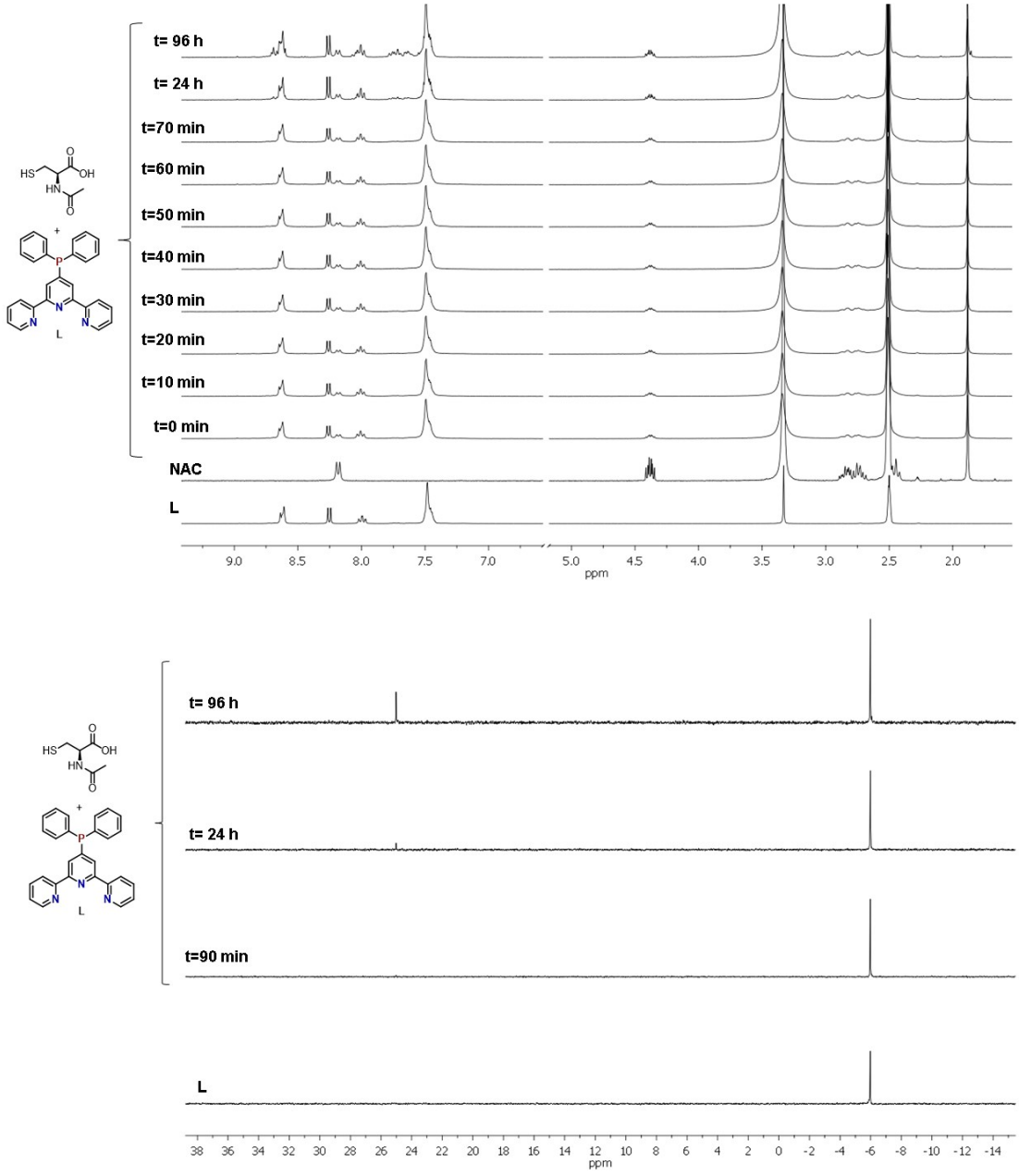

Figure S23: ^{1}H–RMN (300 MHz d_6–DMSO) (up) and $^{31}P\{^{1}H\}$–RMN (121 MHz d_6–DMSO) (bottom) of **L** in presence of NAC at different times.

4 DNA-Binding

4'-PPh_2terpy:

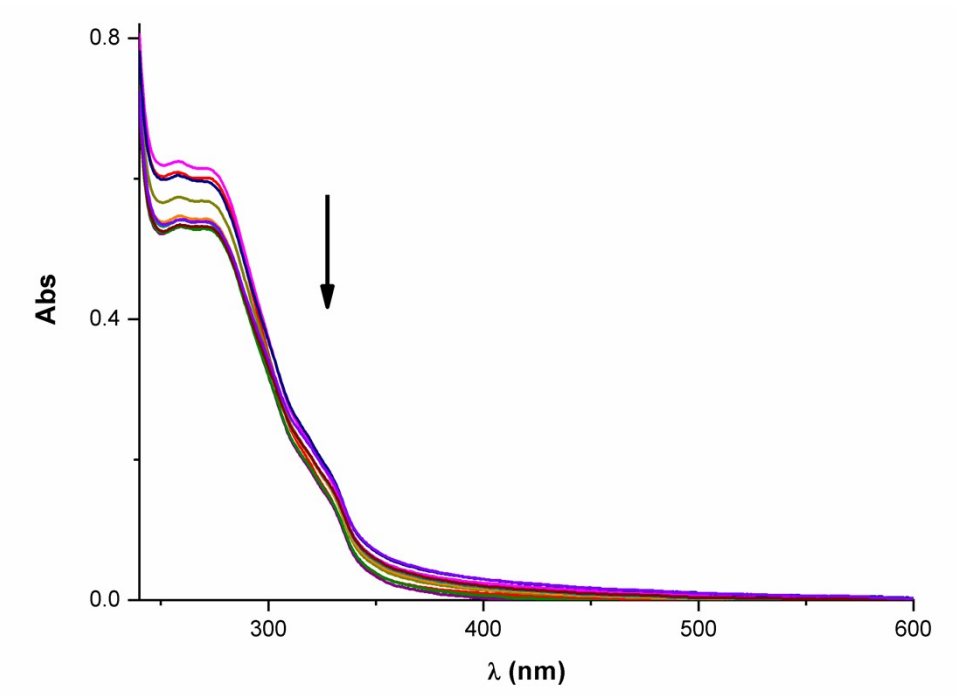

Figure S24: UV-Vis Absorption spectral titration of **4'-PPh_2terpy** in presence of incremental amounts of CT-DNA.

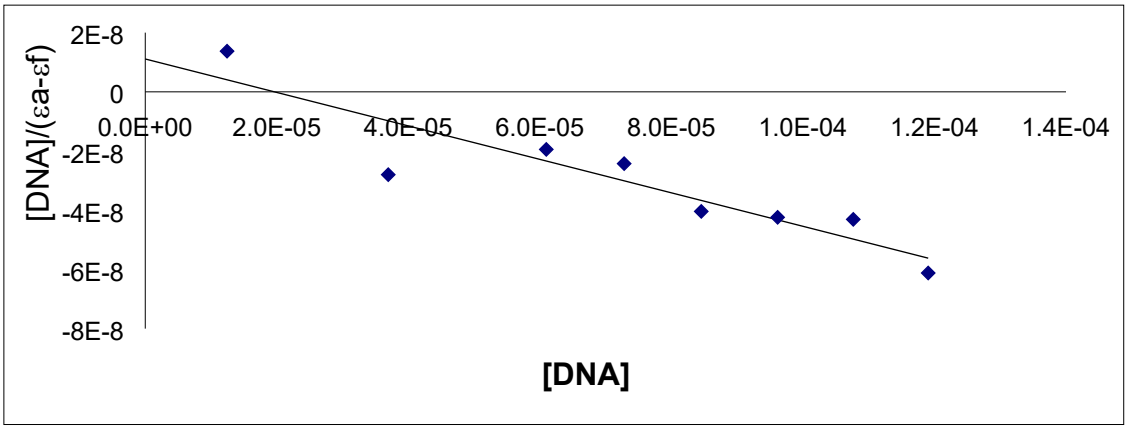

Figure S24a: graphical representation of Wolfe-Shimer equation at 260 nm

[Au($PPh_2(C_6H_4COOH)$)(4′–PPh_2terpy)]BF_4 (**2**)

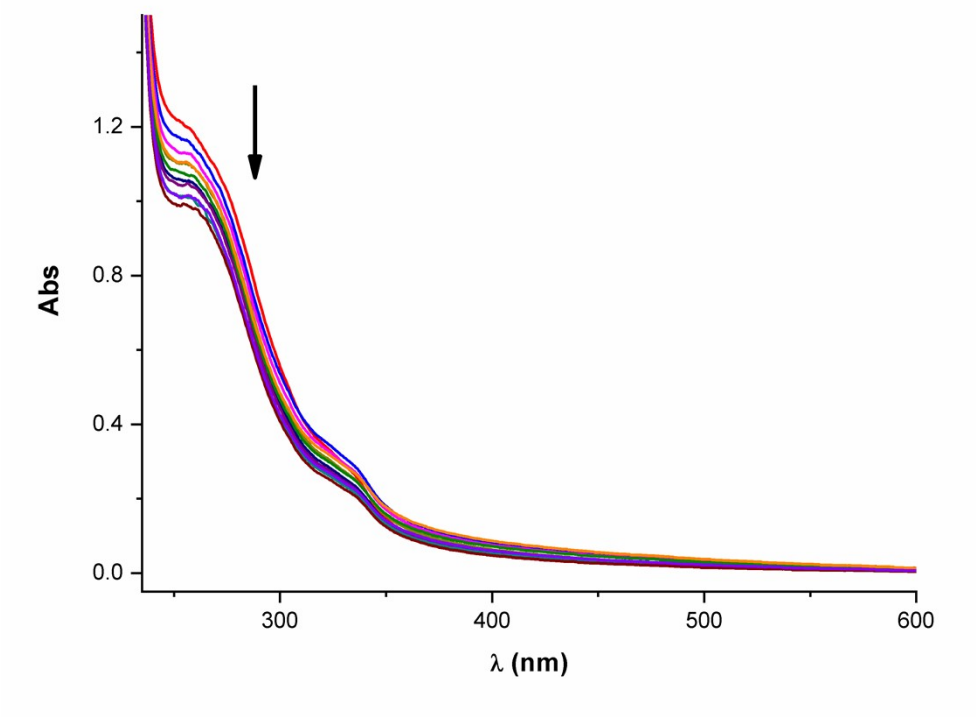

Figure S25: UV-Vis Absorption spectral titration of **2** in presence of incremental amounts of CT-DNA.

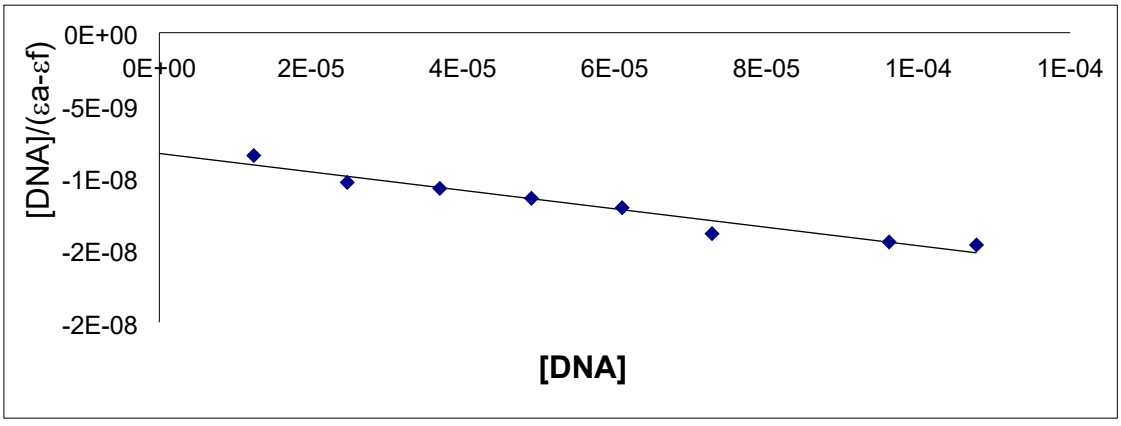

Figure S25a: graphical representation of Wolfe-Shimer equation at 260 nm

[AuCl(4′–PPh_2terpy)] (**3**)

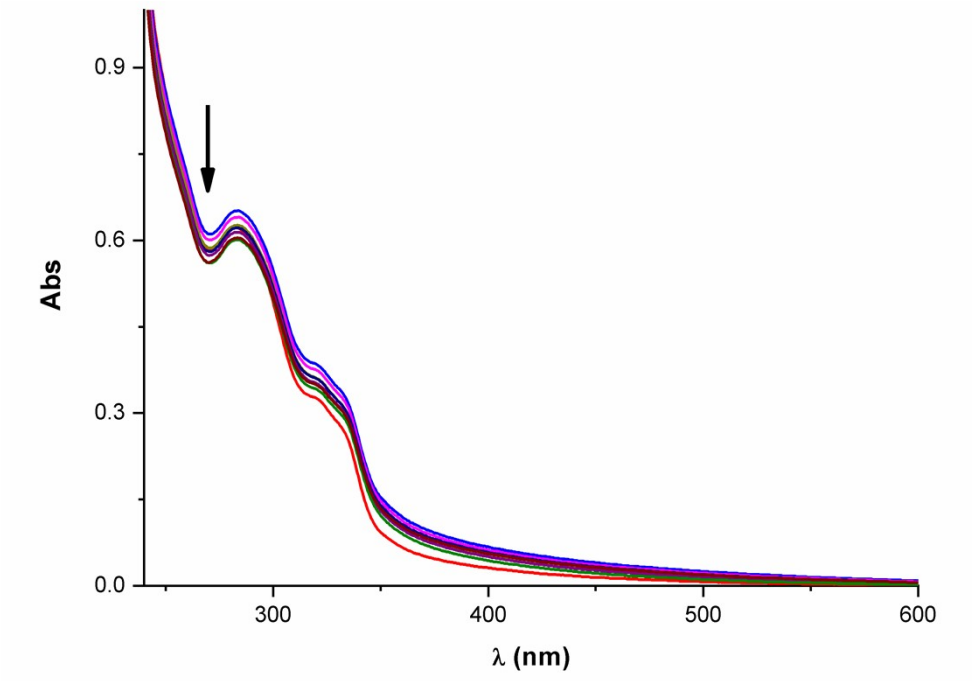

Figure S26: UV-Vis Absorption spectral titration of **3** in presence of incremental amounts of CT-DNA.

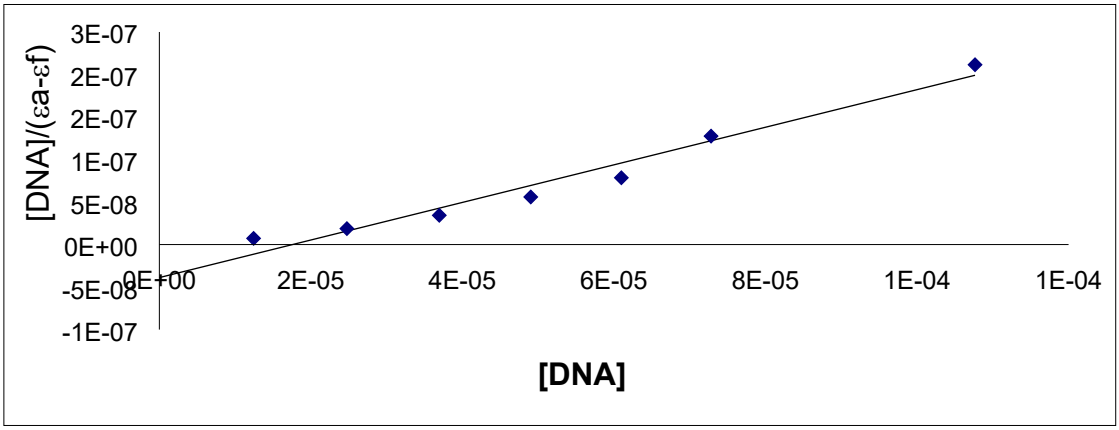

Figure S26a: graphical representation of Wolfe-Shimer equation at 284 nm

[Au(C≡CPh)(4′–PPh_2terpy)] (**4**)

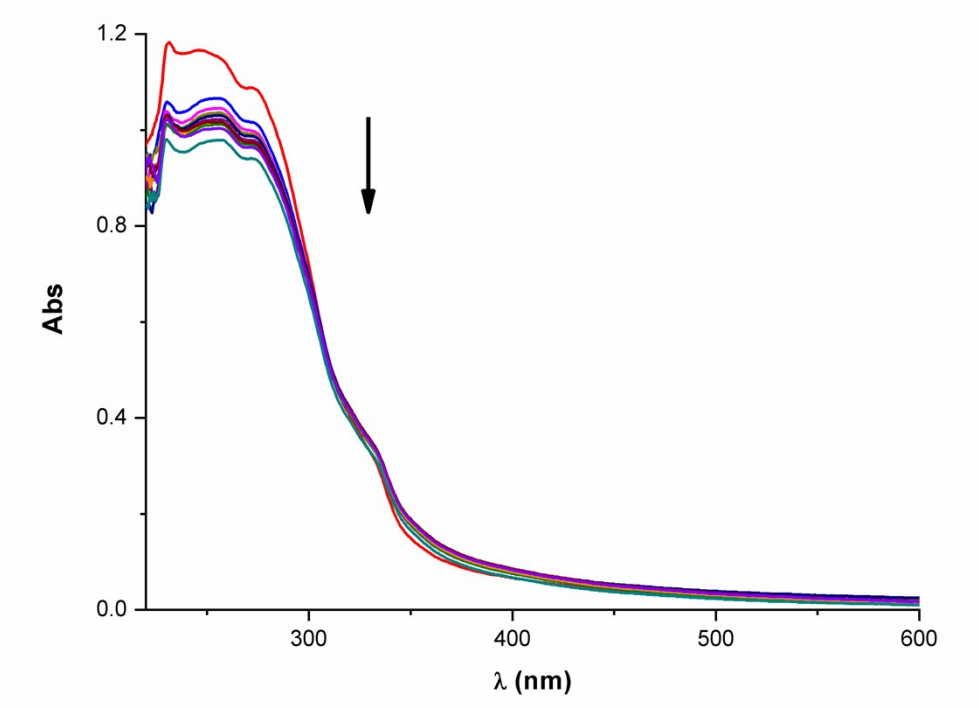

Figure S27: UV-Vis Absorption spectral titration of **4** in presence of incremental amounts of CT-DNA.

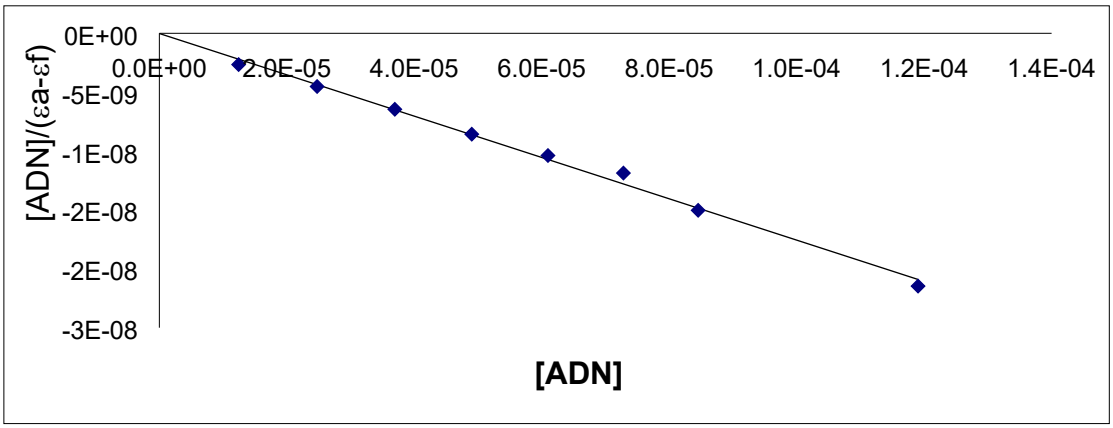

Figure S27a: graphical representation of Wolfe-Shimer equation at 250 nm

[Au(SPyrim)(4´–PPh_2terpy)] (**7**):

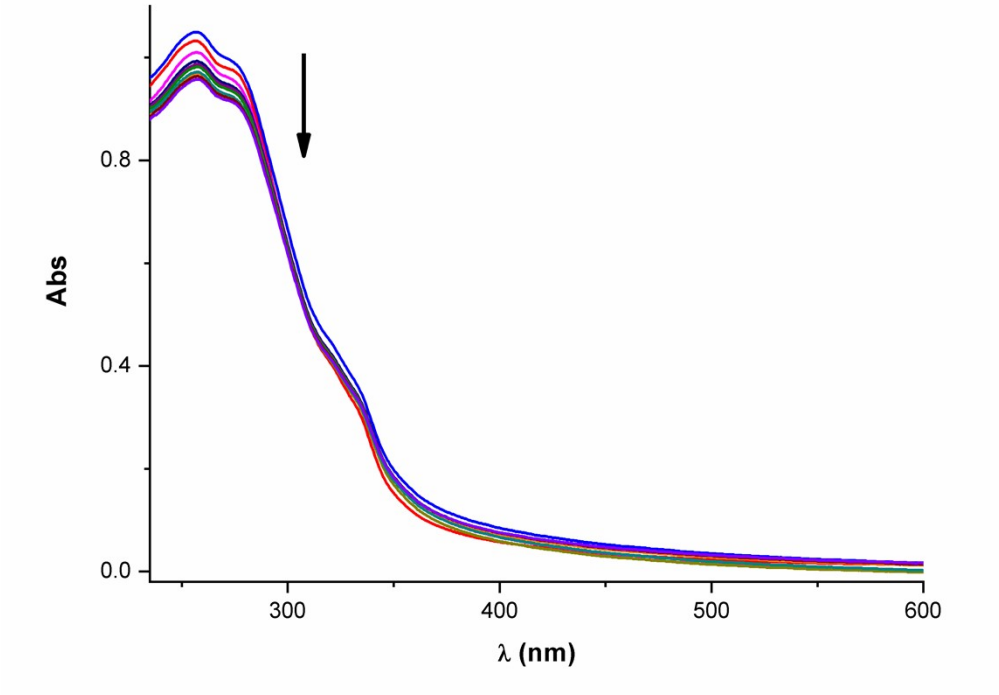

Figure S28: UV-Vis Absorption spectral titration of **7** in presence of incremental amounts of CT-DNA.

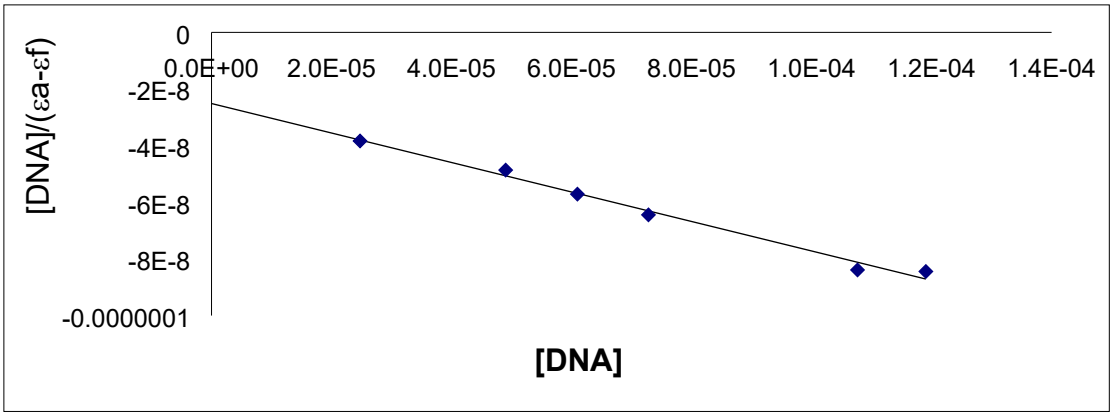

Figure S28a: graphical representation of Wolfe-Shimer equation at 256 nm

5 Fow cytometry

Cell death Studies:

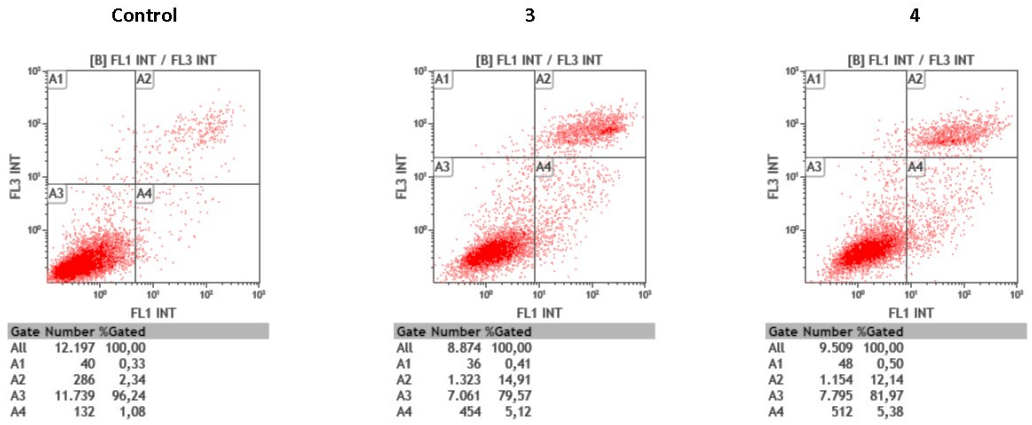

Figure S29: Flow cytometry of MDA-MB-231 cells after incubation for 48 hours with complexes **3** and **4**. Study of cell death mechanism.

Cellular cycle arrest:

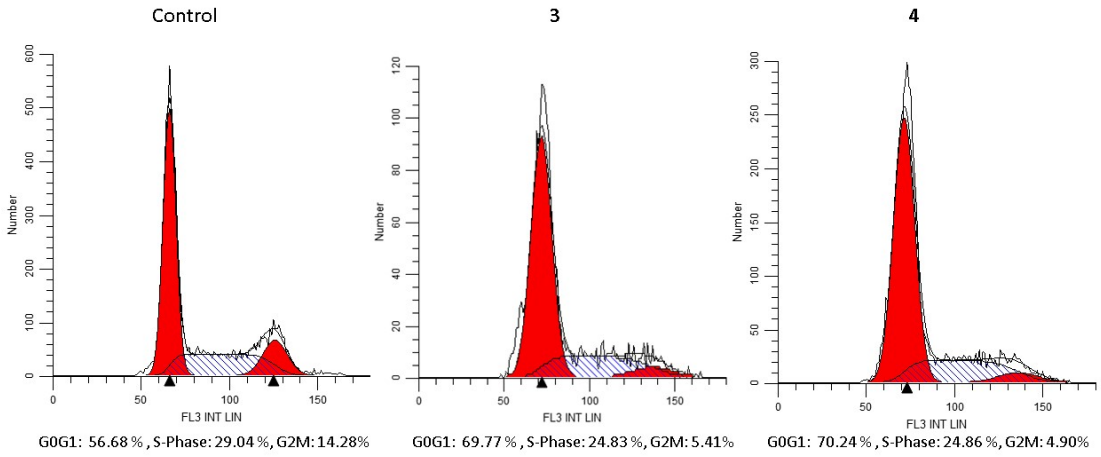

Figure S30: Study DNA contet of MDA-MB-231 cells after incubation for 48 hours with complexes **3** and **4**. Study of cell cycle arrest.

Michocondrial potential (ΔΨ):

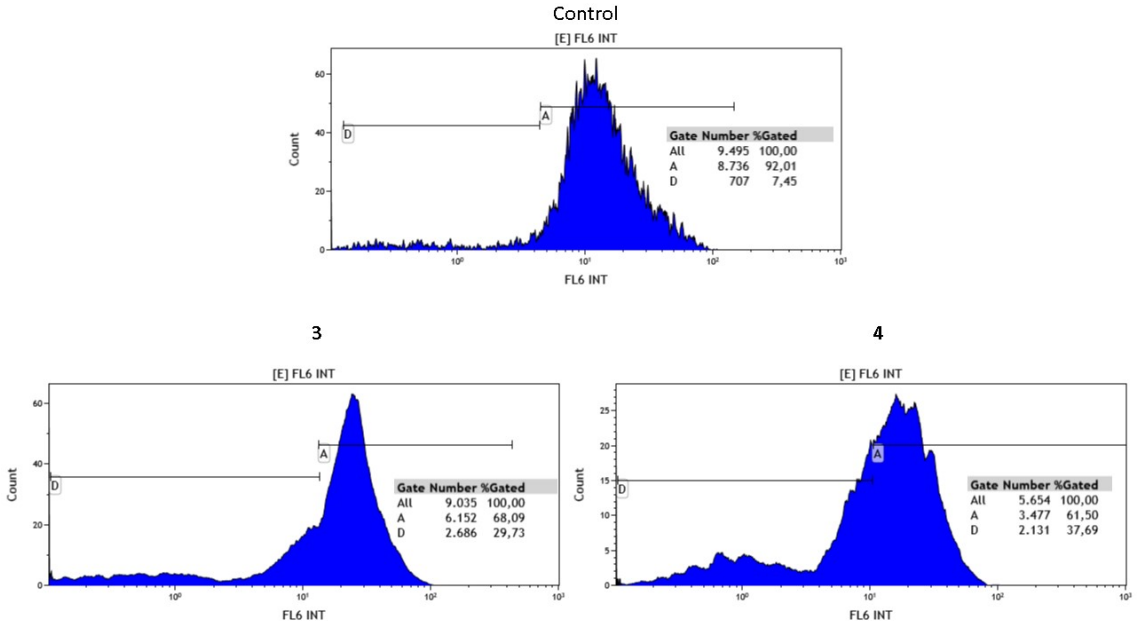

Figure S31: Study of mitochondrial ΔΨ of MDA-MB-231 cells after incubation for 48 hours with complexes **3** and **4**.